Iron Oxide–Gold Core–Shell Nanoparticles: A Review of Spectral Properties for Multimodal Imaging and Targeted Therapy

Dr. E. Martins[1], Dr. T. Becker[1,2], Dr. J. Park[1], Dr. F. Dubois[1], Dr. A. Khan[2], Prof. L. Henderson[1]*

[1] School of Medicine and Public Health, University of Sydney, Sydney, NSW 2006, Australia

[2] Department of Clinical Engineering and Health Technology, Technical University of Munich, Munich 80333, Germany

Abstract

Multimodal nanotheranostics have emerged as a promising tool for combining both therapy and diagnosis of disease into a single nanoplatform. Herein we explore further the optical properties of core-shell, magnetic-plasmonic nanoparticles and their potential for bioapplication in photothermal therapy and diagnostic imaging.

Through modification of commercial magnetite nanoparticles, magnetic-plasmonic, Fe_3O_4-Au, nanoparticles were synthesised with various levels of gold coverage, ranging from a textured core-satellite structure to a full-coverage smooth gold shell with structural verification by transmission electron microscopy. Single-particle broadband dark-field scattering microspectroscopy and solution extinction (absorption) experiments were used to optically characterise the nanoparticles. Interestingly, a significant spectral drift of up to 110 nm was observed between the experimental extinction and scattering.

We note that this spectral drift is potentially advantageous in multimodal applications and demonstrate experimentally that it leads to enhanced photothermal activity away from the wavelengths where imaging via scattering is best. To explore these applications, infrared thermography and laser dark-field microscopy were used to monitor the photothermal activity and imaging, respectively. We propose that the enhanced photothermal response results directly from a reduced competition between absorption and scattering stemming from spectral drift.

I. INTRODUCTION

Both plasmonic and magnetic nanomaterials have individually garnered significant attention over the past decade in a wide range of research fields. When these materials are miniaturised to the nanoscale, interesting phenomena such as superparamagnetism and nanoplasmonics arise. Magnetic nanoparticles exhibiting superparamagnetism have been used as magnetic resonance contrast agents [1], in environmental applications such as magnetic field-assisted bioremediation [2], field-guided drug delivery [3], as nanosensors [4] and as magnetic hyperthermia agents [5]. The ability to externally manipulate and stimulate nanoscaled materials is highly sought after. For example, magnetic-flux-driven drug delivery is possible through the placement of a magnet near the tumour site, maximising the delivery of the nanoparticle-drug conjugates to the site of interest. Plasmonic nanoparticles have been used in

nanosensing [6] most commonly for enhanced analyte detection in surface-enhanced Raman (SERS), as imaging labels [7] and as photothermal agents [8]. Gold is of particular interest for biomedical plasmonic applications as it is chemically inert and less cytotoxic than other plasmonic nanomaterials such as silver and platinum [9]. When these plasmonic nanomaterials are excited at or near their plasmon resonance frequency, the local electron density coherently resonates with the electromagnetic excitation resulting in an enhancement of the local electric field and an intensified optical absorption and scattering cross-section. Furthermore, these mobile carriers dissipate energy through heat generation, which diffuses into the surrounding medium. This process can be utilised to generate localised heating of nanoparticles in tissues to induce targeted cell apoptosis and/or necrosis in a method referred to as plasmonic photothermal therapy. Other applications of thermo-plasmonics include photothermal drug delivery [10], photothermal imaging [11], and photocatalysis [12]–[14]. Traditionally, fluorophores or chromophores are used as labels or tags for visualising or detecting biomolecules. However, these fluorophores suffer from photobleaching, which can lead to doubt in quantitative applications. Plasmonic nanoparticles have been proposed as an alternative thanks to their superior optical properties and photostability and can be functionalised with a surface ligands to target biomolecules as with traditional fluorophores for diagnostic purposes [15]. In-vitro [16], [17] and in-vivo [18], [19] research shows compelling evidence of the efficacy of both plasmonic and magnetic nanoparticles individually; thus, the technology has progressed to clinical studies [20].

A superior nanostructure may be designed which is a hybrid of a magnetic and plasmonic nanoparticle, bringing forth the functionality of each nanoparticle, which may then be combined with both light and magnetic fields for stimulation [21]. Combined magnetic-plasmonic bifunctional nanocomposites have also shown to be successful in-vitro [22], [23] and in-vivo [24] with excellent biocompatibility [25]. Evidently, it is of interest to create a magnetically responsive and optically active nanoparticle to exploit the properties of each material type. Such nanostructures may exist in two distinct forms, as nanocomposites which are hybrid nanoparticles that are not necessarily core-shell gold-coated (such as Janus [26], rod [27] or nanocomposite [28]) and as a pseudospherical core-shell nanoparticle. Here, we focus on the basic physical response of the various stages of magnetic-plasmonic core-shell pseudospherical particles which are important to optimise for dedicated applications such as SERS-based immunoassays and dual magneto-photothermal therapy [29].

In this paper, magnetic-plasmonic nanostructures were synthesised with varied gold coverage, with structural confirmation using transmission electron microscopy (TEM), and their optical activity was studied using extinction and scattering spectroscopy. The absorption, scattering and extinction cross-sections were calculated using COMSOL Multiphysics® finite element analysis models. A spectral offset or drift between the maximum optical absorption and scattering of up to 110 nm is observed experimentally for popcorn-textured thinner Au shell and of ca. 30 nm for smoother and thicker shells, the latter being well replicated by the COMSOL models. Other works have studied this drift theoretically in large solid nanoparticles, silica-metal, core-shell nanoparticles [30]–[32] or indirectly shown a theoretical drift for $BiFeO_3$-Au, core-shell nanoparticles [33]. Conversely, this drift has not been explored

experimentally for Fe_3O_4-Au core-shell nanoparticles before, and neither was its impact on photothermal absorption, which is seen here to be enhanced when a substantial drift exists.

II. RESULTS AND DISCUSSION

Figure 1 shows the various magnetic-plasmonic, Fe_3O_4–Au, nanoparticles synthesised for this work, both in illustration and TEM micrograph. 20 nm diameter commercial oleic acid-capped iron oxide nanoparticles underwent a ligand exchange to amine-terminated silane (stage O, black designation in all graphs in this paper, Figure 1(A)). Gold nanoseeds (Figure 1(B)) were then added to amino functionalised iron oxide nanoparticles, leading to gold seeded iron oxide nanoparticle (stage OS, red in graphs, Figure 1(C)). These gold seeded iron oxide nanoparticles were then exposed to iterative gold reductions, the first reduction (R1, green in graphs, Figure 1(D)), the second reduction (R2, shown in blue, Figure 1(E)) and the third reduction (R3, orange designation in data, Figure 1(F)). This synthesis protocol is detailed in the supplementary information (SI.1) and was adapted from a number of reports in ligand exchange and electroless plating of oxide surfaces [34]–[36]. The TEM images seen on the right of each cartoon depiction is better interpreted by comparing the electron density of Fe_3O_4 (4.89 gm/cc) and Au (15.5 gm/cc) [37]. The contrast seen in TEM is due to this electron density; therefore, gold appears darker than the iron oxide and so, when coated in gold, the iron oxide core is no longer visible. Importantly, at all stages of growth, we verified that the nanoparticles can be magnetically separated, leaving a clear supernatant (see Figure S1 in the supplementary information). A photograph of these nanoparticles at the various stages of synthesis can be seen beside each TEM image. Images in transmitted and reflected white light are shown, with standard vector notation indicating the light direction. In transmitted light, a purple-pink colour can be seen indicative of the gold shell which is not as apparent in reflected light. Aqueous Zeta potential measurements gave the Zeta potential of -0.0 mV for amine-functionalised iron oxide nanoparticles (O), -10.0 mV for the gold seeded iron oxide nanoparticles (Os), -27.3 mV for the gold seeded iron oxide nanoparticles after a gold reduction (R1), -22.4 mV for the iron oxide-gold nanoparticles after two gold reductions (R2) and -22.1 mV for the magnetic-plasmonic nanostructures after three gold reductions (R3); suggesting good colloidal stability for stages R1 to R3.

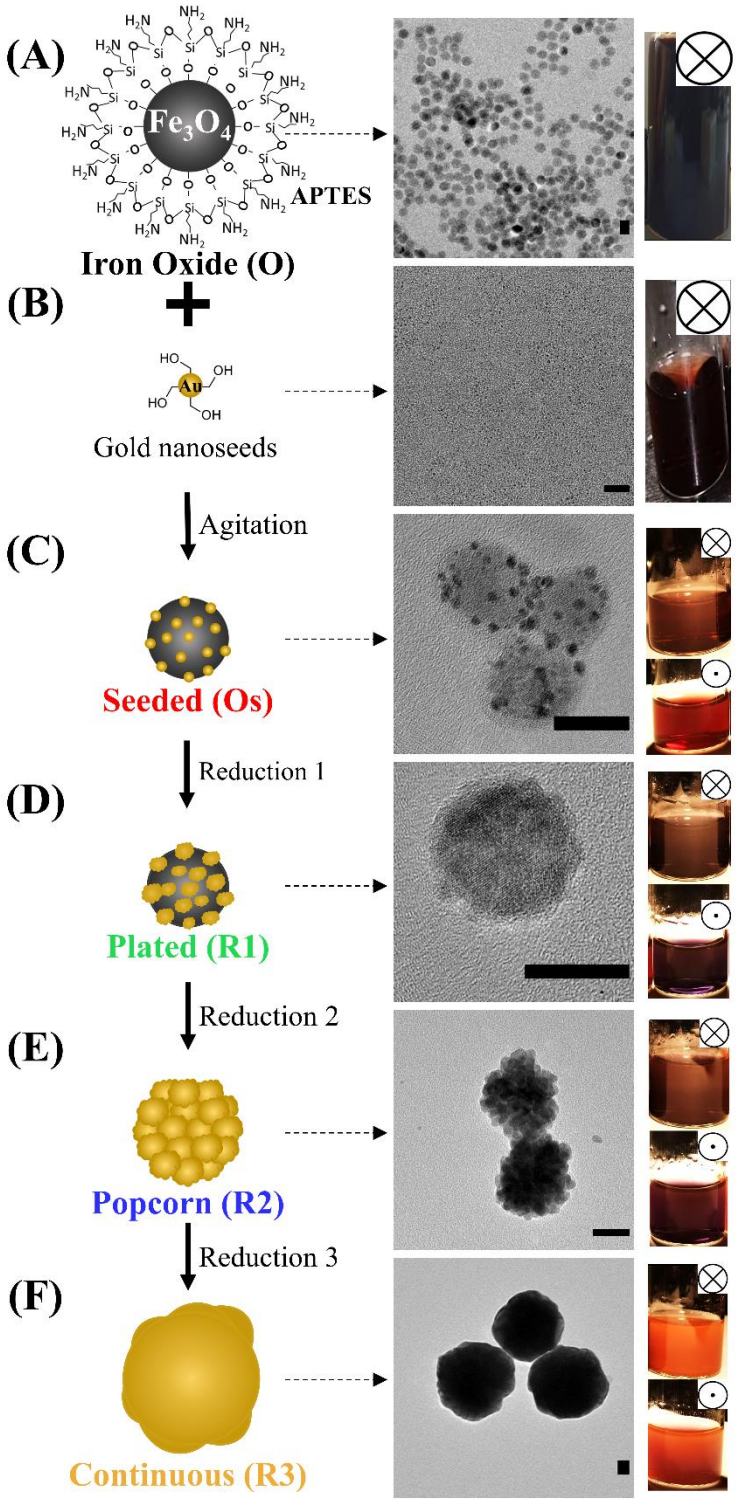

Figure 1: Illustration of the various stages of the magnetic, plasmonic nanoparticles in cartoon form, TEM micrograph and appearance under visible light in solution, in reflected and transmitted light. (A)Amine-functionalised iron oxide nanoparticles with a diameter of 20nm, referred to as "O" throughout this paper. (B) Gold nanoseeds with a diameter of 2-3nm. (C) The combination of stages "O" and gold nanoseeds yields gold-seeded iron oxide nanoparticles, called "Os". (D) After the first reduction, we achieve an electroless-plated textured stage called "R1". (E) After gold reduction, a nanopopcorn stage is attained, which is referred to as "R2" throughout. (F) A continuous gold shell on the iron oxide stage is achieved which is denoted "R3". All scale bars are 20nm.

Dynamic Light Scattering showed an average hydrodynamic diameter of 30.5 nm for R1, 43.2 nm for R2 and 102.8 nm for R3, agreeing with TEM data due to the absence of a surface ligand. Flame Atomic Absorption Spectrometry showed an Au/Fe ratio of 4.3 for Os, 10.7 for R1, 11.6 for R2 and 26.8 for R3. These results further confirm the increase in gold content per nanoparticle from stage Os to R3. By monitoring gold growth through the stages by TEM imaging and maintaining magnetic separability, we deduce that stages R2 and R3 have complete gold coverage and are indeed core-shell particles.

Figure 2 shows the extinction spectra of each magnetic plasmonic nanoparticle growth stage measured in an aqueous solution at a concentration of 20 μg/ml (solid lines). Also seen in Figure 2 are broadband white-light dark-field scattering spectroscopy spectra averaged from several single nanoparticles (dashed lines). The intensity scales for the extinction and absorption are not directly comparable, but each spectra type can be compared for all the sample stages. For further details on experimental techniques and data correction, see supplementary information (SI.1). Both the samples composed of iron oxide (O) and of gold seeded iron oxide nanoparticles (Os) do not exhibit any detectable resonant scattering or extinction (Figure 2(A)) in the studied region. This is in line with the gold nanoseeds grafted to the surface being too small (> 5nm) and known to have a plasmon resonance so broad that it is virtually indiscernible from the background [38]. However, after the iterative gold reductions, distinct scattering and extinction peaks are seen. The averaged scattering (see Figure S2 in the supplementary information for all individual spectra) and extinction peak wavelengths for nanoparticles after one reduction (R1, Figure 2(B)), two reductions (R2, Figure 2(C)) and three reductions (R3, Figure 2(D)) are reproduced in Table 1.

If one defines the experimental spectral drift as the difference between scattering and extinction peak wavelength ($\Delta\lambda = \lambda_{sc} - \lambda_{ext}$), one observes a drift of 67 nm for the first reduction stage of the magnetic-plasmonic nanoparticle (R1), increased after the second reduction stage (R2) to 110 nm and reduced to 33 nm for the third reduction (R3). We note that, although such drift was not reported in earlier experimental studies of Fe_3O_4-Au nanosystems (presumably because single-particle dark-field spectroscopy was not performed), the drift was indeed predicted for core-shell nanoparticles [39].

Table 1: Single-particle scattering peak wavelength (λ_{sca}), solution extinction peak wavelength (λ_{ext}) and corresponding drift.

sample	**λ_{sca} (nm)**	**λ_{ext} (nm)**	**$\Delta\lambda$ (nm)**
R1	625 ± 11	558	67
R2	671 ± 11	561	110
R3	608± 14	575	33

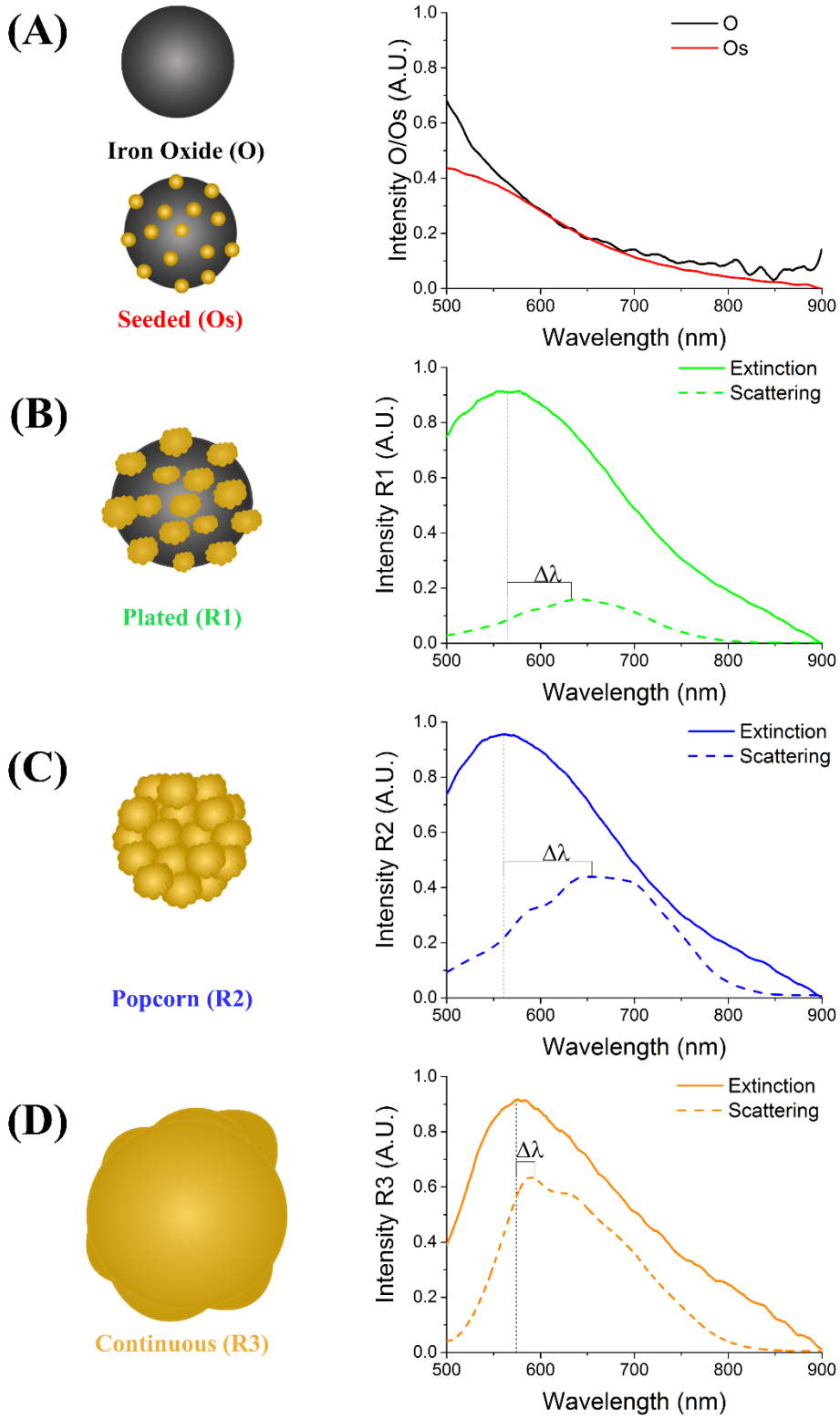

Figure 2: Optical properties of the magnetic-plasmonic nanoparticles at successive gold growth steps. Optical scattering was collected for single particles by dark-field microspectroscopy and optical extinction (predominately absorption) was collected by solution VIS/NIR spectroscopy. (A) Extinction spectra for O (black) and Os (red). (B) Average optical scattering for R1 core-shell (average of 5 individual spectra) (dashed line) and extinction spectrum (solid line). (C) Same for R2. (D) Same for R3. Δλ highlights the spectral drift between extinction and scattering peaks.

The origin of the spectral drift seen in our experiments was further studied by computing absorption and scattering spectra of a single core-shell Fe_3O_4-Au nanoparticle and a single solid gold nanoparticle irradiated by a plane wave using the finite element analysis (FEA) software COMSOL Multiphysics®, details in the supplementary information (SI.2). Figure 3(A) shows the absorption and scattering peak wavelengths of a 20 nm iron oxide core coated by a smooth gold shell of varied thickness (grey curves) and for the same dimensions of solid gold nanoparticle (yellow curves). The dashed and solid lines show scattering and absorption, respectively. The corresponding peak intensities are shown in Figure 3(B). More detailed colour plots of the absorption and scattering at various gold shell thicknesses are shown in the supplementary information (Figure S4).

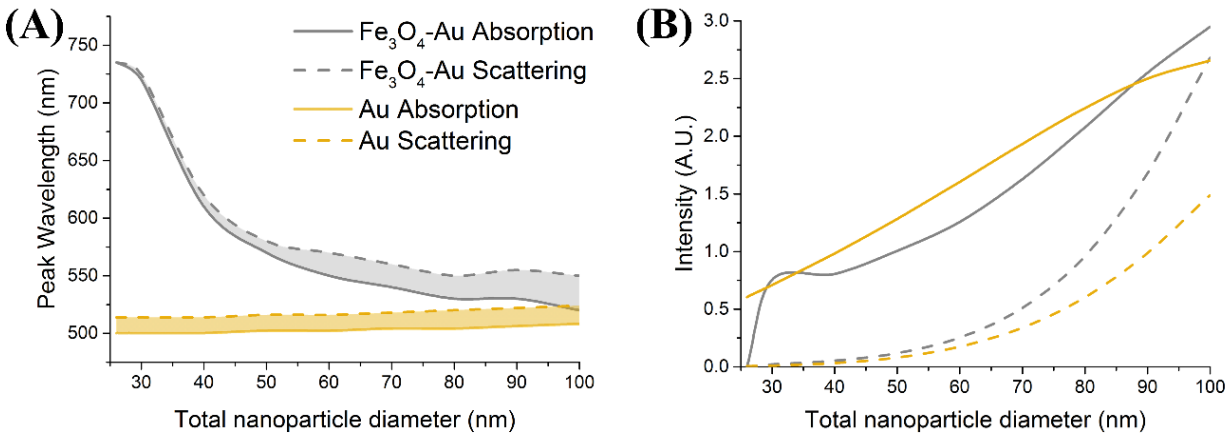

Figure 3: (A) COMSOL Multiphysics®-derived optical absorption (solid line) and scattering (dashed line) peak wavelengths for a spherical 20 nm (diameter) iron oxide core covered with a continuous, smooth gold shell with varied thickness (grey) and for a solid gold nanoparticle (yellow). The spectral drift is marked by the shaded area between the absorption and scattering curves. (B) Corresponding intensities using same colours and line styles.

The shaded areas between the absorption and scattering curves in Figure 3(A) show that the spectral drift for 100 nm particles is ca. 30 nm for core-shell Fe_3O_4-Au, while it is half that value for a plain gold particles. The simulations thus show a fair agreement with R3 in the experiment and confirm the role played by the iron oxide core. However, it is also clear that the simulations do not justify the larger experimental drift for R2 and R1. Given the nature of the seeded growth and the morphology of R1 and R2 confirmed by TEM experiments, we attribute the large drifts to the then natural texturing of the gold shells, which is indeed entirely (and necessarily here) ignored in the model. The same argument was advanced for silica-gold core-shell particles where the roughness was then generated by etching [40]. With the gold roughness decreasing with further reduction at R3, it is thus expected to reach a better match between model and experiment. Rough surfaces of plain gold particles have been observed by others to also exhibit a red-shifting of the plasmon scattering versus smooth particles of the same dimensions, while the extinction spectra in water also showed little dependence on the

roughness [40], in agreement with our own measurements here for Fe_3O_4-Au core-shell nanoparticles.

An important biomedical application of plasmonic and by extension magnetic-plasmonic nanostructures is in photothermal therapy, which is closely related to the optical absorption spectra of nanostructures. It is interesting to investigate how the spectral drift reported above for R1, R2, and R3 relates to the photothermal response of the particles. Here, the photothermal activity of the various magnetic-plasmonic nanostructures was studied by monitoring the temperature increase of aqueous solutions with a fixed concentration of 10 μg/ml of iron oxide upon laser irradiation at 532 and 690 nm with a power density of 1 W/cm^2 spread over a collimated beam of 5 mm diameter. The sample was maintained at room temperature prior to measurement. The change in temperature of the solutions was monitored using a calibrated infrared thermal camera after switching the laser on for 10 minutes and then off for another 10 minutes (see Figure 4).

For the iron oxide cores (i.e. without gold seeds or shell, O), we observe the smallest increase in temperature and very little difference when the wavelength is changed from 532 to 690 nm. The seeded particles (Os) exhibit a similar response but exhibits a ca. 20% increase in temperature at 690 nm. The small changes versus O can be explained from the limited amount of gold on the particles after seeding. For the thickest gold shell tested here, R3, we observe a temperature increase that is twice that of O and Os at 532 nm with a decrease of ca. 20% at 690 nm. Overall, these particles show limited dependence on the excitation wavelength used.

Conversely, the nanoparticles R1 and R2 show a temperature increase enhanced ca. 2.5× versus O and Os at 532 nm, as well as a clear wavelength dependence with a decrease in maximum temperature upon irradiation at 690 nm to values nearer to those measured for O and Os. Thus, we observe that, although R1 and R2 carry a smaller mass of gold than R3, they are more efficient in converting the incident radiation into heat. We propose that the large reduction in scattering at 532 nm for R1 and R2 justifies the enhancement in photothermal response as the probability that photons are absorbed is not competing with elastic scattering. Conversely, for R3, the lesser drift implies that the scattering remains substantial both at 532 and 690 nm.

A dual theranostic modality can also benefit from the larger spectral drift of the textured R1 and R2. Indeed Figure 2 and Figure 4 together show that the photothermal response is less where the scattering is larger, so that a better separation between therapy and imaging (diagnostic) is possible, if the imaging is conducted near the scattering peak whereas the photothermal therapy is delivered near the absorption peak.

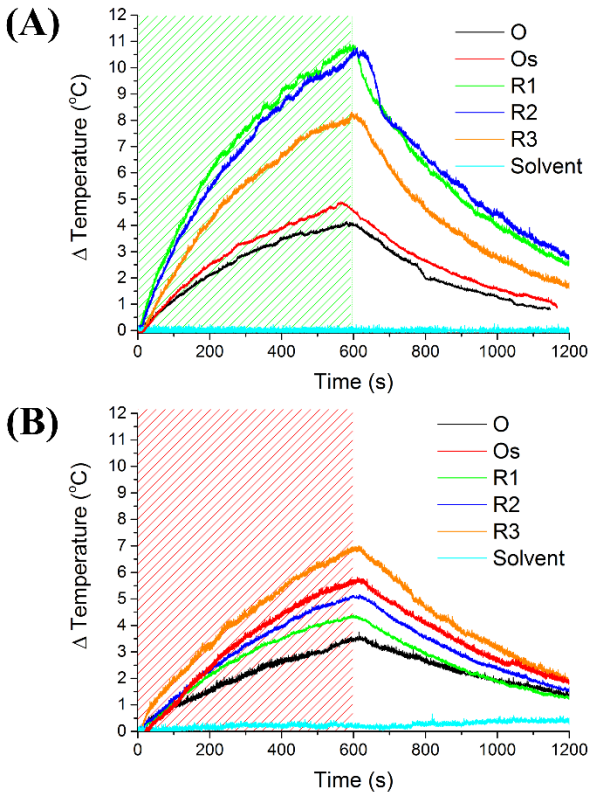

Figure 4: (A) Temperature variations for solutions of Fe_3O_4-Au core-shell (O, Os, R1, R2, R3, and water solution) measured by infrared thermography. The solution were at room temperature at 0 s, exposed to a 532 nm laser beam (1W/cm^2) during 600s, and with the laser exposure stopped during another 600 s. (B) Same using 690nm excitation.

Dark-field imaging is typically conducted with a high angle broadband white light source illumination (NA 1.3, oil) and a lower numerical aperture (NA 0.9, air) collection, affording wide-field visualisation. For improved sensitivity and reduced imaging time, it is also possible to use laser excitation. This technique of laser dark-field imaging of the nanoparticles could be translated to bioimaging applications using the magnetic-plasmonic nanoparticles as labels. This would be a monochromatic, coherent version of standard dark-field bioimaging [41], without the complication of dual-beam imaging as is the case with photothermal bioimaging [42]. Here, we selected to use low NA excitation (ca. NA 0.5, air) with higher NA dark field collection (NA 0.8, air) as this is simpler to implement by addition of a beam stop in the detection path and from the long working distances involved, although the scheme provides here a much lower spatial resolution. Figure 5 shows dark-field images of R1 and R3 at 540 and 620 nm, recording the same area for each. In agreement with the broadband scattering spectra in Figure 2(B, D), the scattered intensity is seen to increase for both R1 and R3, when the wavelength is changed from 540 to 620 nm. This confirms that textured particles such as R1 are indeed better imaged at these longer wavelengths where the photothermal heating is relatively inefficient and that these particles are good candidates for a dual theranostics approach where the efficient a diagnostic based on imaging and a therapy based on photothermal heating are spectrally resolved with minimum overlap.

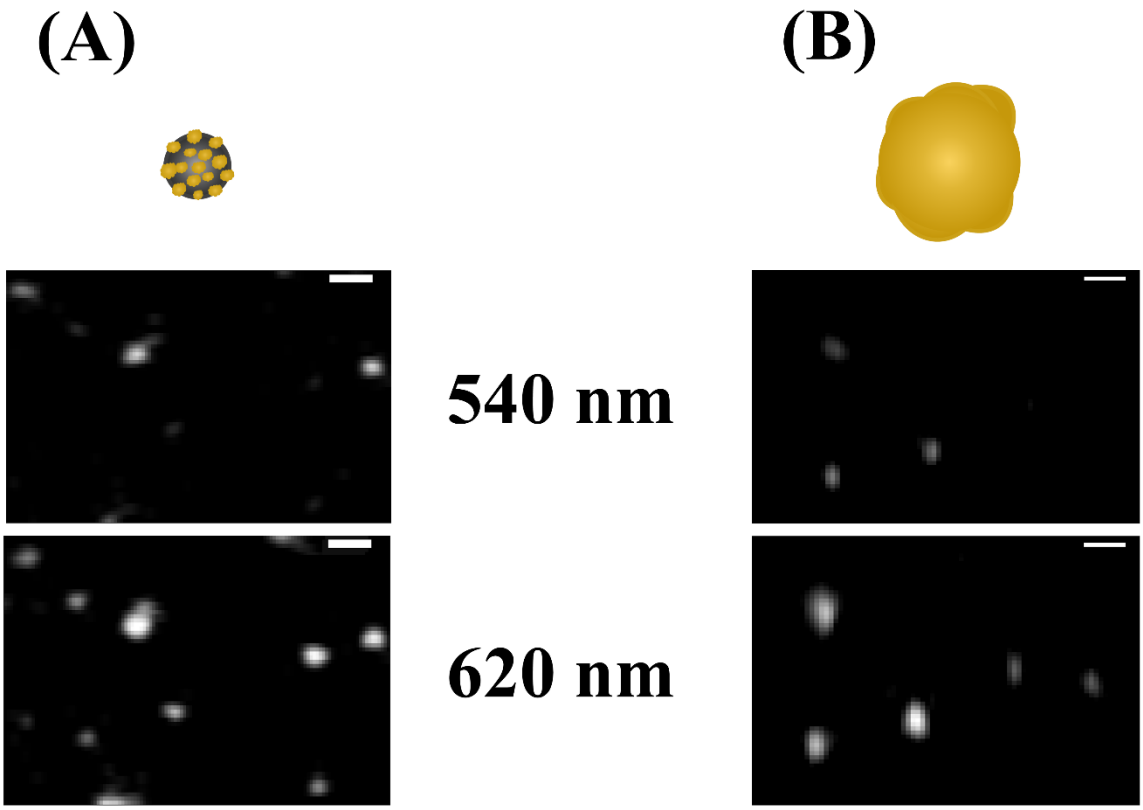

Figure 5: Laser dark-field imaging of magnetic-plasmonic nanoparticles after one (R1) and three (R3) reductions at both 540 nm and 620 nm.

III. CONCLUSIONS

Fe_3O_4–Au core-shell nanoparticles were synthesised through the modification of commercial Fe_3O_4 nanoparticles. We prepared and investigated a core-satellite structure (Os) obtained by seeding with gold nanoseeds, followed by successive steps of gold reduction (R1, R2, R3) onto these Os particles. From Os to R3, the gold shell evolved from a seed-textured roughness towards smoother shells, as confirmed by TEM. We report a significant drift (up to 110 nm) between extinction and scattering peaks, especially for R1 and R2, where the surface texturing remains high. At later gold growth stages, such as for R3, the drift is ca. 30 nm in line with models of smooth gold shells on iron oxide cores. Remarkably, R1 and R2 show a high spectral dependence in their photothermal response upon laser irradiation as well as a significant enhancement versus R3. These effects are attributed to the remarkably low scattering shown by R1 and R2 at 532 nm where their absorption remains high as a consequence of the drift. We conclude that such seeded core-shell nanoparticles are promising candidates for combined therapy and diagnostics with the possibility to spectrally separate the wavelengths where photothermal response and scattering efficiency are their highest.

IV. REFERENCES

[1] X. Yin et al., "Large T1 contrast enhancement using superparamagnetic nanoparticles in ultra-low field MRI," Sci. Rep., vol. 8, no. 1, Dec. 2018.

[2] S. He, L. Zhong, J. Duan, Y. Feng, B. Yang, and L. Yang, "Bioremediation of wastewater by iron Oxide-Biochar nanocomposites loaded with photosynthetic bacteria," Front. Microbiol., vol. 8, no. MAY, May 2017.

[3] V. V. Mody, A. Cox, S. Shah, A. Singh, W. Bevins, and H. Parihar, "Magnetic nanoparticle drug delivery systems for targeting tumor," Applied Nanoscience (Switzerland), vol. 4, no. 4. Springer Nature, pp. 385–392, 01-Apr-2014.

[4] T. A. P. Rocha-Santos, "Sensors and biosensors based on magnetic nanoparticles," TrAC - Trends in Analytical Chemistry, vol. 62. Elsevier B.V., pp. 28–36, 01-Nov-2014.

[5] E. A. Périgo et al., "Fundamentals and advances in magnetic hyperthermia," Applied Physics Reviews, vol. 2, no. 4. American Institute of Physics Inc., 01-Dec-2015.

[6] J. N. Anker, W. P. Hall, O. Lyandres, N. C. Shah, J. Zhao, and R. P. Van Duyne, "Biosensing with plasmonic nanosensors," Nat. Mater., vol. 7, no. 6, pp. 442–453, Jun. 2008.

[7] S.-H. Wang, C.-W. Lee, M.-Y. Pan, S.-Y. Hsieh, F.-G. Tseng, and P.-K. Wei, "Chromatogram Analysis on Revealing Aggregated Number and Location of Gold Nanoparticles Within Living Cells," Plasmonics, vol. 10, no. 4, pp. 873–880, Aug. 2015.

[8] X. Huang, I. H. El-Sayed, W. Qian, and M. A. El-Sayed, "Cancer cell imaging and photothermal therapy in the near-infrared region by using gold nanorods," J. Am. Chem. Soc., vol. 128, no. 6, pp. 2115–2120, 2006.

[9] P. V. Asharani, Y. Lianwu, Z. Gong, and S. Valiyaveettil, "Comparison of the toxicity of silver, gold and platinum nanoparticles in developing zebrafish embryos," Nanotoxicology, vol. 5, no. 1, pp. 43–54, Mar. 2011.

[10] H. Takahashi, Y. Niidome, and S. Yamada, "Controlled release of plasmid DNA from gold nanorods induced by pulsed near-infrared light," Chem. Commun., no. 17, pp. 2247–2249, May 2005.

[11] J. He, J. Miyazaki, N. Wang, H. Tsurui, and T. Kobayashi, "Label-free imaging of melanoma with nonlinear photothermal microscopy," Opt. Soc. Am., vol. 40, no. 7, pp. 1141–1144, 2015.

[12] Z. Chehadi, J. S. Girardon, M. Capron, F. Dumeignil, and S. Jradi, "Thermoplasmonic-induced energy-efficient catalytic oxidation of glycerol over gold supported catalysts using visible light at ambient temperature," Appl. Catal. A Gen., vol. 572, pp. 9–14, Feb. 2019.

[13] M. Mutlu et al., "Thermoplasmonic Ignition of Metal Nanoparticles," Nano Lett., vol. 18, no. 3, pp. 1699–1706, Mar. 2018.

[14] G. Baffou, Thermoplasmonics: Heating metal nanoparticles using light. 2017.

[15] C. Loo, A. Lowery, N. Halas, J. West, and R. Drezek, "Immunotargeted nanoshells for integrated cancer imaging and therapy," Nano Lett., vol. 5, no. 4, pp. 709–711, Apr. 2005.

[16] S. Lotfi, A. Bahari, and S. Mahjoub, "In vitro biological evaluations of Fe 3 O 4 compared with core–shell structures of chitosan-coated Fe 3 O 4 and polyacrylic acid-coated Fe 3 O 4 nanoparticles," Res. Chem. Intermed., 2019.

[17] S. R. Koohi et al., "Plasmonic photothermal therapy of colon cancer cells utilising gold

nanoshells: An in vitro study," in IET Nanobiotechnology, 2018, vol. 12, no. 2, pp. 196–200.

[18] E. B. Dickerson et al., "Gold nanorod assisted near-infrared plasmonic photothermal therapy (PPTT) of squamous cell carcinoma in mice," Cancer Lett., vol. 269, no. 1, pp. 57–66, Sep. 2008.

[19] C. J. Zhou et al., "Folate-conjugated Fe3O4 nanoparticles for in vivo tumor labeling," Trans. Nonferrous Met. Soc. China (English Ed., vol. 23, no. 7, pp. 2079–2084, Jul. 2013.

[20] A. C. Anselmo and S. Mitragotri, "A Review of Clinical Translation of Inorganic Nanoparticles," AAPS J., vol. 17, no. 5, pp. 1041–1054, Sep. 2015.

[21] N. D. Thorat et al., "Physically stimulated nanotheranostics for next generation cancer therapy: Focus on magnetic and light stimulations," Applied Physics Reviews, vol. 6, no. 4. p. 041306, Dec-2019.

[22] J. Kim et al., "Designed fabrication of multifunctional magnetic gold nanoshells and their application to magnetic resonance imaging and photothermal therapy," Angew. Chemie - Int. Ed., vol. 45, no. 46, pp. 7754–7758, Nov. 2006.

[23] J. Lee et al., "Multifunctional magnetic gold nanocomposites: Human epithelial cancer detection via magnetic resonance imaging and localized synchronous therapy," Adv. Funct. Mater., vol. 18, no. 2, pp. 258–264, 2008.

[24] N. S. Elbialy, M. M. Fathy, and W. M. Khalil, "Doxorubicin loaded magnetic gold nanoparticles for in vivo targeted drug delivery," Int. J. Pharm., vol. 490, no. 1–2, pp. 190–199, 2015.

[25] Y. Li et al., "Biocompatibility of Fe3O4@Au composite magnetic nanoparticles in vitro and in vivo.," Int. J. Nanomedicine, vol. 6, pp. 2805–2819, 2011.

[26] C. Jin, Y. Qu, M. Wang, J. Han, Y. Hu, and R. Guo, "Aqueous Solution-Based Fe3O4 Seed-Mediated Route to Hydrophilic Fe3O4-Au Janus Nanoparticles," Langmuir, vol. 32, no. 18, pp. 4595–4601, May 2016.

[27] D. Zhou et al., "Visible light-driven, magnetically steerable gold/iron oxide nanomotors," Chem. Commun., vol. 53, no. 83, pp. 11465–11468, 2017.

[28] K. C. F. Leung et al., "Gold and iron oxide hybrid nanocomposite materials," Chemical Society Reviews, vol. 41, no. 5. pp. 1911–1928, 07-Mar-2012.

[29] A. Espinosa, R. Di Corato, J. Kolosnjaj-Tabi, P. Flaud, T. Pellegrino, and C. Wilhelm, "Duality of Iron Oxide Nanoparticles in Cancer Therapy: Amplification of Heating Efficiency by Magnetic Hyperthermia and Photothermal Bimodal Treatment," ACS Nano, vol. 10, no. 2, pp. 2436–2446, 2016.

[30] W. Chaabani, A. Chehaidar, and J. Plain, "Comparative Theoretical Study of the Optical Properties of Silicon/Gold, Silica/Gold Core/Shell and Gold Spherical Nanoparticles," Plasmonics, vol. 11, no. 6, pp. 1525–1535, Dec. 2016.

[31] J. Zhu, J. J. Li, and J. W. Zhao, "Tuning the wavelength drift between resonance light absorption and scattering of plasmonic nanoparticle," Appl. Phys. Lett., vol. 99, no. 10, p. 101901, Sep. 2011.

[32] X. Zhang, S. Ye, X. Zhang, and L. Wu, "Optical properties of SiO2@M (M = Au, Pd, Pt) core-shell nanoparticles: Material dependence and damping mechanisms," J. Mater. Chem. C, vol. 3, no. 10, pp. 2282–2290, 2015.

[33] A. Chehaidar and M. Hadded, “Scattering and absorption of light by homogeneous BiFeO3 and hybrid BiFeO3/Au core/shell spherical nanoparticles: A computational study,” Opt. Mater. (Amst)., vol. 95, Sep. 2019.

[34] K. Davis, B. Cole, M. Ghelardini, B. A. Powell, and O. T. Mefford, “Quantitative Measurement of Ligand Exchange with Small-Molecule Ligands on Iron Oxide Nanoparticles via Radioanalytical Techniques,” Langmuir, vol. 32, no. 51, pp. 13716–13727, Dec. 2016.

[35] S. Sun et al., “Monodisperse MFe 2 O 4 (M = Fe, Co, Mn) Nanoparticles,” J. Am. Chem. Soc., vol. 126, no. 1, pp. 273–279, 2004.

[36] S. J. Oldenburg, R. D. Averitt, S. L. Westcott, and N. J. Halas, “Nanoengineering of optical resonances,” Chem. Phys. Lett., vol. 288, no. 2–4, pp. 243–247, May 1998.

[37] “Mineralogy Database.” [Online]. Available: http://webmineral.com/. [Accessed: 06-Sep-2019].

[38] M. M. Alvarez, J. T. Khoury, T. G. Schaaff, M. N. Shafigullin, I. Vezmar, and R. L. Whetten, “Optical absorption spectra of nanocrystal gold molecules,” J. Phys. Chem. B, vol. 101, no. 19, pp. 3706–3712, May 1997.

[39] J. Zhu, J. J. Li, and J. W. Zhao, “Tuning the wavelength drift between resonance light absorption and scattering of plasmonic nanoparticle,” Appl. Phys. Lett., vol. 99, no. 10, p. 6755, 2011.

[40] J. Rodríguez-Fernández, A. M. Funston, J. Pérez-Juste, R. A. Álvarez-Puebla, L. M. Liz-Marzán, and P. Mulvaney, “The effect of surface roughness on the plasmonic response of individual sub-micron gold spheres,” Phys. Chem. Chem. Phys., vol. 11, no. 28, pp. 5909–5914, 2009.

[41] C. Menzel et al., “The spectral shift between near- and far-field resonances of optical nano-antennas,” Opt. Express, vol. 22, no. 8, p. 9971, 2014.

[42] Z. Guan et al., “Simultaneous Imaging and Selective Photothermal Therapy through Aptamer-Driven Au Nanosphere Clustering,” J. Phys. Chem. Lett., vol. 10, no. 2, pp. 183–188, 2019.

V. ACKNOWLEDGEMENTS

The authors wish to thank Ms Bridget Hogan for conducting atomic absorption spectroscopy. This work was supported by Science Foundation Ireland (SFI) centre CÚRAM, the European Regional Development Fund (Grant Number 13/RC/2073), Marie Sklodowska-Curie Grant Agreement No. 751903, and SFI CDA award 13CDA2221.

